Research on the influence of sampling on three-dimensional surface shape measurement

Nao-sheng Qiao[1,2,*], and Xue Shang[2]

(1 International College, Hunan University of Arts and Science, Changde 415000, P.R.China)

(2 *Mathematics and physics Science College, Hunan University of Arts and Science, Changde 415000, P.R.China)*

**Corresponding author, E-mail: naoshengqiao@163.com*

Abstract: In order to accurately measure the three-dimensional surface shape of object, the influence of sampling on it was studied. Firstly, on the basis of deriving spectra expressions through Fourier transform, the generation of CCD pixels was analyzed and its expression was given. Then, basing on the discrete expression of deformation fringes obtained after sampling, its Fourier spectrum expression was derived, resulting in an infinitely repeated "spectra island" in the frequency domain. Finally, on the basis of using a low-pass filter to remove high-order harmonic components and retaining only one fundamental frequency component, the signal strength is reconstructed by inverse Fourier transform. A method of reducing the sampling interval, i.e. reducing the number of sampling points per fringe, was proposed to increase the ratio m between the sampling frequency and the fundamental frequency of the grating, so as to more accurately reconstruct the object surface shape under the condition of $m > 4$. The basic principle was verified through simulation and experiment. In the simulation, the sampling intervals are 8 pixels, 4 pixels, 2 pixels and 1 pixel, respectively, the maximum absolute error values obtained in the last three situations are 88.80%, 38.38% and 31.50% of the first situation, respectively, and the corresponding average absolute error values are 71.84%, 43.27% and 32.26% of which. It can be seen that the smaller the sampling interval, the better the recovery effect. And in the experiment, taking

收稿日期：2023-01-31；**修订日期**：2024-02-25
基金项目：湖南省教育厅科学研究重点项目（No. 22A0484）；国家自然科学基金（No. 12104150）
Supported by Key Scientific Research Project of Hunan Provincial Department of Education (No. 22A0484); National Natural Science Foundation of China (No. 12104150)

in press

the same 4 sampling intervals as in the simulation can also lead to the same conclusions. The simulated and experimental results show that reducing the sampling interval can improve measurement accuracy of object surface shape and achieve better reconstruction results.

Key words: three-dimensional surface shape measurement; sampling interval; spectra overlapping; pixel; measurement accuracy

抽样对三维形貌测量的影响研究

乔闹生 [1,2,*]，尚雪 [2]
（1 湖南文理学院 国际学院，湖南 常德 415000）
（2 湖南文理学院 数理学院，湖南 常德 415000）

摘 要：为了精确地测量物体的三维形貌，研究了抽样对它的影响。首先，在经傅里叶变换推出频谱表达式的基础上，分析了CCD像元的产生并给出了其表达式。然后，经抽样得到离散的变形条纹表达式，并推导出了其傅里叶频谱表达式，从而得到了频域内无限重复的“频谱岛”。最后，在利用低通滤波器滤除高级频谱成份后仅保留其中一个基频成份的基础上，由逆傅里叶变换来恢复信号强度；提出了减小抽样间隔即减小每根条纹抽样点数的方法来增大抽样频率与光栅基频的比值 m，使之在满足 m > 4 的条件下更准确地恢复物体的三维形貌。用仿真和实验对基本原理进行了验证。在仿真中，抽样间隔分别取8 pixels、4 pixels、2 pixels、1 pixel，后三种情况所得到的最大绝对误差值分别为第一种情况下的88.80%、38.38%和31.50%，平均绝对误差值分别为第一种情况下的71.84%、43.27%和32.26%。可见，抽样间隔越小，恢复的效果越好。在实验中，取与仿真中相同的4次抽样间隔，也能得到与仿真中相同的结论。结果表明：减小抽样间隔可提高三维形貌的测量精度，得到的恢复效果更好。

关键词：三维形貌测量；抽样间隔；频谱混叠；像元；测量精度
中图分类号：O438.2　　**文献标识码：**A

1. Introduction

The three-dimensional surface shape measurement based on grating projection is widely applied in various fields such as computer vision, physical simulation, automatic detection, biology and medicine. It has many advantages such as high speed, high accuracy, non-contact, automation, etc[1-20]. Many scholars in the word have conducted research on it and achieved good results. For example, to reduce phase measurement errors caused by measuring glossy surfaces, Zhou *et al* proposed a pixel by pixel combination multi intensity matrix projection method. It has significantly reduced the

In Press

numbers of projection operations and time consumption[4]. Due to the influence of too many projected patterns on phase unwrapping, Yang *et al* proposed a high-speed measurement method suitable for three-dimensional shape which use only three high-frequency internal shift phase modes (70 cycles), which improved measurement accuracy and speed, and obtained wrapping phase and fringe order[5]. In the use of gray code method, Lu *et al* proposed a method based on staggered gray code light, which successfully avoided step errors without projecting additional gray code modes[6]. Due to overexposure in optical three-dimensional measurement, phase information cannot be obtained well, Feng *et al* put forwarded a high reflective surface measurement method based on pixel by pixel modulation, thereby the measurement speed and accuracy was improved greatly[7].

During the measurement process, due to the fact that the CCD (Charge Coupled Device) imaging system is not a general translation invariant system, but a sampling imaging system with discrete characteristics, it will cause image distortion, resulting in spectra overlapping during the transformation process, and thus bringing errors to the three-dimensional surface shape measurement[8-10]. In order to reduce or eliminate these errors and improve its accuracy, many scholars have proposed better measurement methods[11-13]. Due to the nonlinear effect of CCD on high-power laser wavefront detection, Du *et al* proposed a method to reduce or eliminate spectra overlapping caused by CCD nonlinear effect by increasing spatial carrier frequency[11]. Due to the important role played by the nonlinearity of scientific level CCD in experimental processing, Cheng *et al* used two different schemes to experimentally test the nonlinear characteristics of CCD and achieved good experimental results[12]. Owing to the nonlinear effects of CCD, spectra overlapping can occur in complex optical three-dimensional surface shape measurement. Qiao *et al* used dual-frequency grating projection method eliminated the nonlinear effects of CCD and improved measurement[13].

in Press

Now the influence of sampling on the three-dimensional surface shape measurement is studied, and the detailed reasoning and analysis are provided on its basic principles. In order to effectively validate the basic principle analysis, the simulations and experiments are conducted, and the better results are achieved.

2. Principle analysis

The measurement system schematic diagram is shown in Fig. 1, P_1P_2 is the projector optical axis, L_0 is the distance between the optical center I_2 of CCD imaging system and the reference plane, A and C are the points located on the reference plane, and D is the point on the object surface, h is the distance from D to the reference surface.

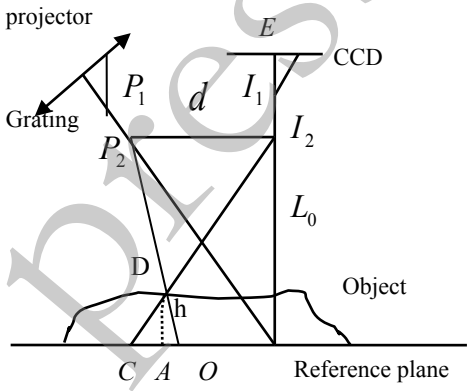

Fig.1 Measurement system schematic diagram

By projecting the grating onto the surface of a three-dimensional object, the signal strength obtained by the CCD imaging system can be expressed as follows

$$g(x,y) = r(x,y)\sum_{n=-\infty}^{\infty} a_n \exp\{j[2\pi n f_0 x + n\phi(x,y)]\}$$
$$= \sum_{n=-\infty}^{\infty} q_n(x,y)\exp(j2\pi n f_0 x) \quad (1)$$

in Press

where $r(x,y)$ is non-uniform reflectivity of object surface, n is Fourier series, a_n is n-order Fourier coefficient of $g(x,y)$, f_0 is the fundamental frequency of grating. And $\phi(x,y)$ is phase of object, where $q_n(x,y)=a_n r(x,y)\exp[jn\varphi(x,y)]$.

By performing the fast Fourier transform on Eq. (1) and using π phase shifting technology[14] to eliminate the zero-order spectra components present in the frequency domain, the spectra expression which contains the object height information can be obtained as follows

$$\begin{aligned} G(f_x,f_y) &= \int_{-\infty}^{\infty}\int_{-\infty}^{\infty} g(x,y)\exp[-j2\pi(f_x x+f_y y)]dxdy \\ &= \sum_{n=-\infty}^{\infty} Q_n(f_x-nf_0,f_y-nf_0)+\sum_{n=-\infty}^{\infty} Q_n^*(f_x-nf_0,f_y-nf_0) \end{aligned} \tag{2}$$

where $G(f_x,f_y)$ and $Q_n(f_x,f_y)$ are the spectra obtained by Fourier transform of $g(x,y)$ and $q_n(x,y)$, respectively, $Q_n^*(f_x,f_y)$ is the conjugate complex of $Q_n(f_x,f_y)$.

Due to the fact that CCD is an array composed of several small pixels arranged neatly and tightly with a certain geometric size, each CCD has approximately hundreds of thousands or even millions of pixels[15]. Let the pixel shape be a rectangle, which presented by the function $rect(x/\Delta x, y/\Delta y)$, where Δx and Δy present the dimensions of the pixel in the direction of x-axis and y-axis, respectively. Therefore, the signal strength of each pixel can be represented as the convolution of $g(x,y)$ and $rect(x/\Delta x, y/\Delta y)$, its expression is as follows

$$g'(x,y)=g(x,y)*rect(\frac{x}{\Delta x},\frac{y}{\Delta y}) \tag{3}$$

in press

Using a comb function to sample Eq. (3), the discrete deformation fringe expression is obtained as follows

$$\begin{aligned} g''(x,y) &= g'(x,y)comb(\frac{x}{\Delta x_1},\frac{y}{\Delta y_1}) \\ &= [g(x,y)*rect(\frac{x}{\Delta x},\frac{y}{\Delta y})]comb(\frac{x}{\Delta x_1},\frac{y}{\Delta y_1}) \end{aligned} \tag{4}$$

where Δx_1 and Δy_1 present the sampling intervals of the fringes in the direction of x-axis and y-axis, respectively.

The spectrum function obtained by performing Fourier transform on Eq. (4) is:

$$\begin{aligned} G''(f_x,f_y) &= G(f_x,f_y)\sum_{n_x=-\infty}^{+\infty}\sum_{n_y=-\infty}^{+\infty}\delta(f_x-\frac{n_x}{\Delta x_1},f_y-\frac{n_y}{\Delta y_1}) \\ &= \frac{1}{sl}\sum_{n_x=-\infty}^{+\infty}\sum_{n_y=-\infty}^{+\infty}\sin c(\frac{n_x\pi}{s})\sin c(\frac{n_y\pi}{l})Q(f_x-f_0-\frac{n_x}{\Delta x_1},f_y-f_0-\frac{n_y}{\Delta y_1}) \end{aligned} \tag{5}$$

where n_x and n_y present pixel points on x-axis and y-axis, respectively, $s=\Delta x_1/(\Delta x+\Delta x')$ and $l=\Delta y_1/(\Delta y+\Delta y)$ present the number of sampling points for each fringe in the corresponding direction, respectively, and $\Delta x'$ and $\Delta y'$ present the pixel spacing in the corresponding direction, respectively.

It is thus clear that the spectra of the sampling function is the infinite repetition for the spectra of the primitive continuous function in the frequency domain, it is commonly known as "spectra island"[15]. As a result, in addition to f_0, the higher-order spectral components such as second-order and third-order are also generated.

Due to the useful information containing changes of object height is contained within f_0 of the spectra, it must design a suitable low-pass filter to gain the f_0 and remove the high-order spectra component.

in Press

The low-pass filter is actually a modulation system of a point spread function, its filtering process is the convolution process of the spectrum function and the point spread function $G_1(f_x, f_y)$. And $G_1(f_x, f_y)$ in the frequency domain is presented by a Gaussian filter as follows

$$G_1(f_x, f_y) = \frac{1}{2\pi}\exp(-\frac{f_x^2 + f_y^2}{2\delta^2}) \tag{6}$$

where δ presents the standard deviation of the filter related to the defocus degree.

The spectra signal obtained through system defocusing is

$$G'''(f_x, f_y) = G''(f_x, f_y) \otimes G_1(f_x, f_y) \tag{7}$$

By filtering, the higher-order harmonics can be well separated from f_0, so that only one of the $(1/sl)\sin c(\pi/s)\sin c(\pi/l)Q(f_x - f_0 - 1/\Delta x_1, f_y - f_0 - 1/\Delta y_1)$ is retained after filtering out the higher-order harmonic components.

Then the inverse Fourier transform is enforced on Eq. (7) to reconstruct the signal strength taken by the CCD imaging system. The measurement system outputs the n-th sine fringe image, which is obtained by CCD system, as shown below

$$\hat{g}(x, y) = F^{-1}[G'''(f_x, f_y)] = \sum_{k=-\infty}^{\infty} \hat{A_k} \cos\{k[2\pi f_0 x + \phi(x, y) + \delta_n]\} \tag{8}$$

where $F^{-1}[\cdot]$ presents inverse Fourier transform, $\hat{A_k}$ presents the Fourier coefficient of $\hat{g_n}(x, y)$, and δ_n presents the phase-shift amount, $\delta_n = 2n\pi/n_1$, $n = 1, 2, \mathrm{L}, n_1$.

When the n-step phase-shift method is used, we can gain the phase as follows

in press

$$\phi^{\wedge}(x,y)=\tan^{-1}\left[\frac{\sum_{n=1}^{N}g^{\wedge}{}_{n}(x,y)\sin(\delta_n)}{\sum_{n=1}^{N}g^{\wedge}{}_{n}(x,y)\cos(\delta_n)}\right] \tag{9}$$

where $\phi^{\wedge}(x,y)$ is wrapped phase.

Under the condition of telecentric projection optical path, considering $L_o >> h(x,y)$ in the real measurement conditions, $h(x,y)$ and $\phi^{\wedge}(x,y)$ will satisfy the relations

$$h(x,y)=-\frac{L\phi^{\wedge}(x,y)}{2\pi f_0 d} \tag{10}$$

It has been discussed in literature [15] that in order to ensure the separation of the f_0 from other periodic spectra components and the separation of spectra components during the same periodic, it must satisfy the sampling condition $m>4$ (where $m=\Delta f/f_0$, Δf presents sampling frequency). This can avoid overlapping between the f_0 and the higher-order spectra components, so as to accurately reconstruct the object shape measured, otherwise it is difficult to reconstruct it.

Lastly, according to $s=\Delta x_1/(\Delta x+\Delta x^{'})$ and $l=\Delta y_1/(\Delta y+\Delta y^{'})$, combining the relationship $\Delta f_x=1/\Delta x_1$ as well as $\Delta f_y=1/\Delta y$ between sampling frequency and sampling interval, it can be obtained that

$$\begin{cases} m_x=\dfrac{1}{\Delta x_1 f_0}=\dfrac{1}{s(\Delta x+\Delta x^{'})f_0} \\ m_y=\dfrac{1}{\Delta y_1 f_0}=\dfrac{1}{l(\Delta y+\Delta y^{'})f_0} \end{cases} \tag{11}$$

where m_x and m_y present the ratio of the sampling frequency in the direction of x-axis and y-axis to f_0, respectively.

in press

It can be seen that the method of reducing the sampling interval, i.e., the number of sampling points of per-fringe, to increase the m, can be used to increase the measurement accuracy of object surface shape.

3. Simulation and experiment

Simulation and experiment are executed to validate the basic principle analysis.

3.1 Simulation

We perform computer simulation verification on the analysis of basic principles. Assuming that the geometric parameter of the measurement system is $L_0/d = 4$. And the simulated object surface shape is shown in Fig. 2, with a size of 512×512 *pixels*.

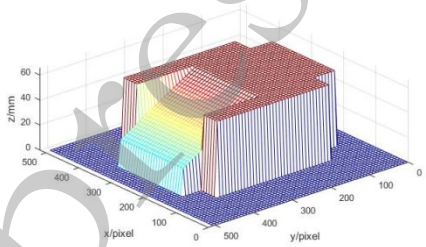

Fig. 2 The simulated object surface shape

We project a digital projector onto a simulated object and use a CCD camera system to obtain deformation fringes. If 40 fringes are taken, then $f_0 = 40/512$ fringe/pixel. Using MATLAB to process the fringes, the sampling intervals of both x-axis direction and y-axis direction are 8 pixels, thus, $m = 1.6000$ can be obtained from Eq. (11). Reducing the sampling interval of the fringes to 0.5 times of which the original sampling interval, i.e. the sampling interval is 4 pixels. From $s = \Delta x_1/(\Delta x + \Delta x')$ and $l = \Delta y_1/(\Delta y + \Delta y')$, it can be seen that the number of sampling points for each fringe is 0.5 times that of the original, and from Eq. (11), $m = 3.2000$ can be

in Press

obtained. It can be seen that both of the two situations do not satisfy the sampling condition $m > 4$. The obtained spectra diagrams are shown in Fig. 3 (a) and 3(b), respectively.

Then, we make the sampling points of each fringe $1/4$ and $1/8$ times of the original, i.e. the sampling interval is 2 pixels and 1 pixel, respectively. $m = 6.4000$ and $m = 12.8000$ can be obtained respectively, indicating that the sampling condition $m > 4$ is satisfied. The obtained spectra diagrams are shown in Fig. 3 (c) and 3(d), respectively.

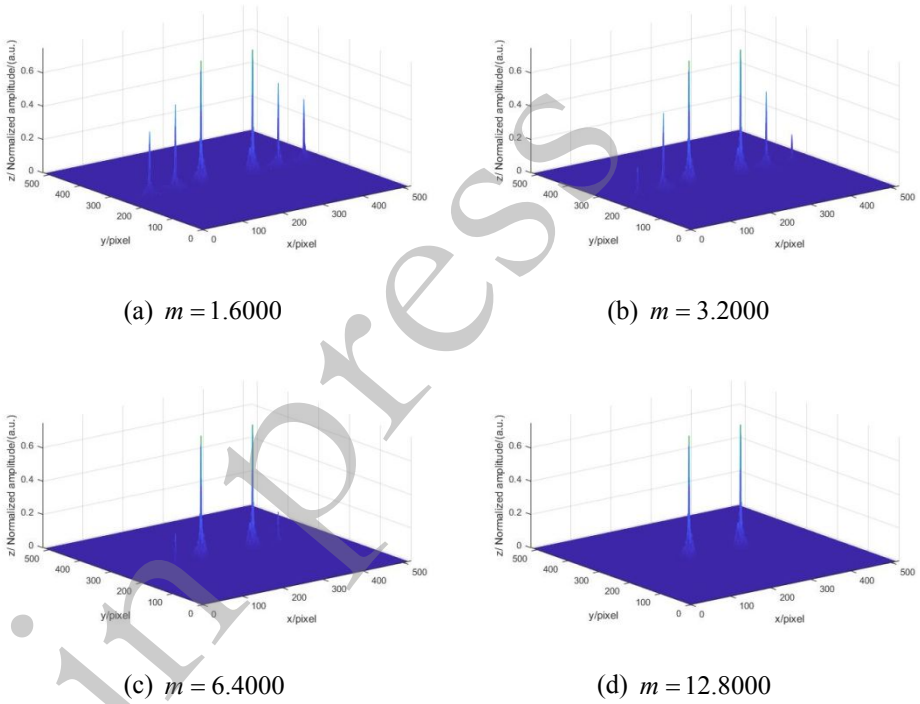

(a) $m = 1.6000$ (b) $m = 3.2000$

(c) $m = 6.4000$ (d) $m = 12.8000$

Fig. 3 The spectra diagrams

In Figs. 3 (a) and 3(b), because the sampling condition $m > 4$ is not satisfied, the components of f_0 in the spectra diagrams are overlapped with the higher-step frequency components. But in Figs. 3 (c) and 3(d), the corresponding frequency components are separated because the sampling

in press

condition is satisfied. In the four sub-figures, the smaller the number of sampling points, the larger the m, and the better the separation effect.

In the above four situations, the errors of the surface shape between the reconstructed object and the simulated object is shown in Fig. 4.

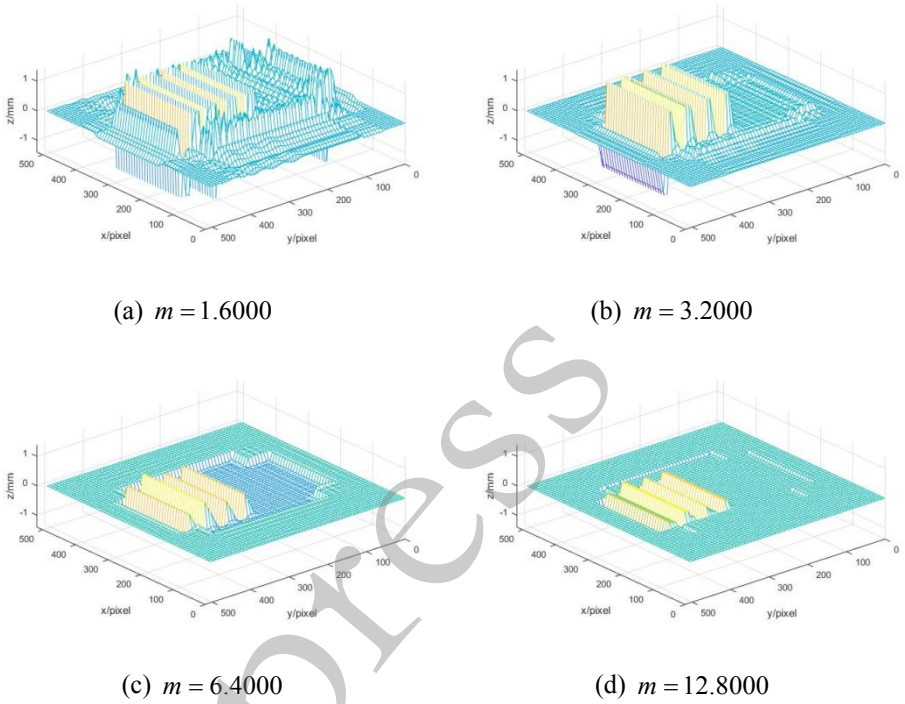

(a) $m = 1.6000$ (b) $m = 3.2000$

(c) $m = 6.4000$ (d) $m = 12.8000$

Fig. 4 The errors of the surface shape between reconstructed object and simulated object

The maximum absolute error value (MAEV) and average absolute error value (AAEV) of each sub-image in Fig. 4 are shown in Tab. 1. The MAEV obtained from the last three sampling intervals are 88.80%, 38.38% and 31.50%, and the AAEV are 71.84%, 43.27% and 32.26%, respectively, of the first sampling interval.

Tab. 1. Error between reconstructed object and simulated object

Sampling interval	8 pixels	4 pixels	2 pixels	1 pixel
MAEV	1.3246	1.1762	0.5084	0.4173
AAEV	0.4758	0.3418	0.2059	0.1535

In Press

As can be seen from Fig. 4 and Tab. 1, when sampling condition $m > 4$ is not satisfied, the object surface shape is difficult to reconstruct or has relatively larger errors. On the contrary, the error is relatively small. The larger the m, the smaller the error, but it is necessary to improve the resolution of the CCD imaging system.

3.2 Experiment

To further validate the impact of CCD imaging system sampling on three-dimensional surface shape measurement, an actual measurement experiment of a hemispherical object has been carried out. The simple experimental device system is shown in Fig. 5, which uses a digital projector and a low distortion CCD camera.

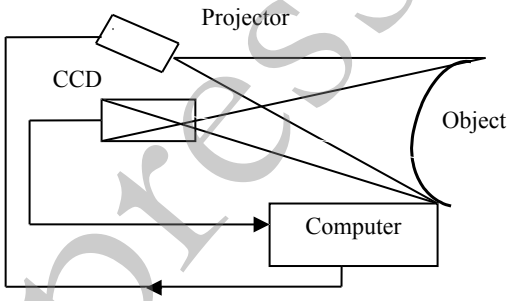

Fig. 5 The simple experimental device system

We use the same method as computer simulation to obtain the deformation fringes of the experimental object. And we take 600×480 pixels and 40 fringes, the fundamental frequencies are $f_x = 40/600$ fringe/pixel and $f_y = 40/480$ fringe/pixel, respectively. Using MATLAB to process the fringes, the sampling intervals of two directions are 8 pixels. From Eq. (11), $m_x = 1.8750$ and $m_y = 1.5000$ can be obtained.

Using the same method as computer simulation, reduce the sampling interval of the fringes to 0.5 times that of the original fringes, that is, change

in press

the sampling interval to 4 pixels. Similarly, $m_x = 3.7500$ and $m_y = 3.0000$ can be obtained from Eq. (11).

It can be seen that both of the above situations do not satisfy the sampling condition $m > 4$. The reconstructed object surface shapes are shown in Fig. 6 (a) and 6(b), respectively.

Making the sampling intervals for each fringe in the direction of x-axis and y-axis to 2 pixels and 1 pixel, respectively, then $m_x = 5.6250$, $m_y = 4.5000$ and $m_x = 7.5000$, $m_y = 6.0000$ can be obtained, respectively. Both of the situations satisfy the sampling condition $m > 4$. The reconstructed object surface shapes are shown in Fig. 6 (c) and 6(d), respectively.

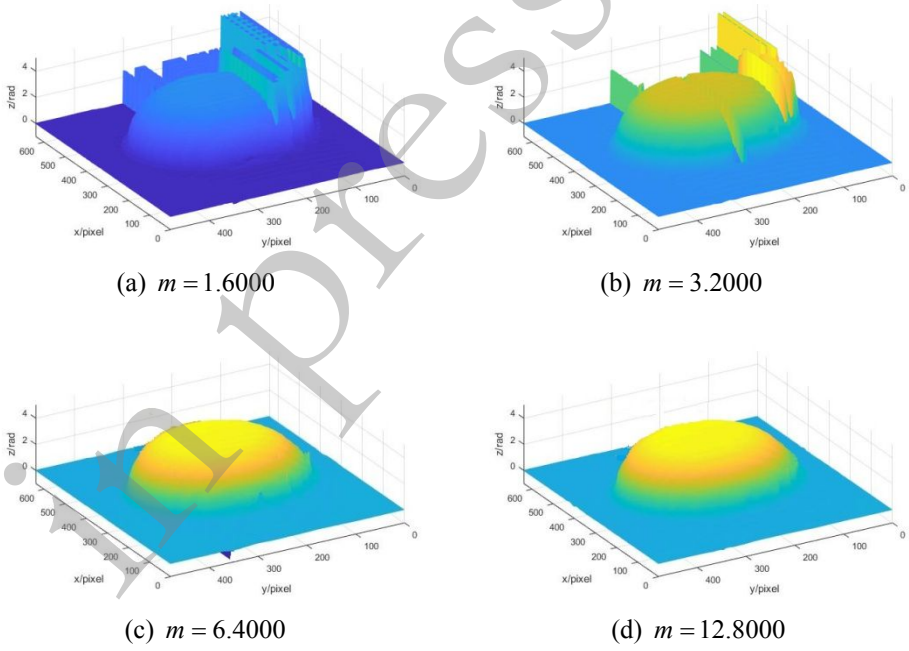

(a) $m = 1.6000$ (b) $m = 3.2000$

(c) $m = 6.4000$ (d) $m = 12.8000$

Fig. 6 Results of object surface shape reconstructed under different sampling conditions

Comparing the experimental reconstruction results of the four sub-images in Fig. 6, the same conclusions can be drawn as the computer simulation results mentioned above.

4. Conclusions

in press

Due to the impact of sampling on the three-dimensional surface shape measurement accuracy, the basic principles of spectra overlapping, spectra separation and measurement accuracy caused by sampling were analyzed and discussed.

Using the comb function to sample the signal intensity of each pixel in the CCD, and the discrete deformation fringes are obtained. After Fourier transform of the deformation fringes, the "spectra island" will be generated in the frequency domain. When we use the method of reducing the CCD sampling interval, i.e. increase the sampling frequency to satisfy the sampling condition $m > 4$, the adjacent " spectra islands" will not overlap with the f_0, thus we can obtain better reconstruction of the three-dimensional shape.

When the sampling interval of pixels is reduced, it will cause the ratio m to increase, and when the sampling condition are satisfied, the larger the m, the better the three-dimensional shape recovery of object, but it is necessary to further improve the resolution of the CCD imaging system.

In the computer simulation and practical experiment, the smaller the sampling interval for each fringe, i.e. the fewer sampling points, the better the reconstruction effect of the surface shape of object. If the sampling condition $m > 4$ is satisfied, it will effectively reconstruct the three-dimensional shape of the object.

in press

References:

[1] MA X, NI H, LU M, *et al*. A measurement method for three-dimensional inner and outer surface profiles and spatial shell uniformity of laser fusion capsule[J]. *Optics & Laser Technology*, 2021, 134: 106601.

[2] FAN H, QI L, CHEN C, *et al*. Underwater optical 3-D reconstruction of photometric stereo considering light refraction and attenuation[J]. *IEEE Journal of Oceanic Engineering*, 2021, 47(1): 46-58.

[3] 杨建柏, 赵建, 孙强. 基于交比不变性的投影仪标定[J]. 中国光学(中英文), 2021, 14(2): 320-328.

YANG J B, ZHAO J, SUN Q. Projector calibration based on cross ratio invariance[J]. *Chinese Optics*, 2021, 14(2): 320-328.

[4] ZHOU P, WANG H Y, LAI J L, *et al*. 3D shape measurement for shiny surface using pixel-wise composed fringe pattern based on multi-intensity matrix projection of neighborhood pixels[J]. *Optical Engineering*, 2021, 60(10): 104101-104101.

[5] YANG S, HUANG H, WU G, *et al*. High-speed three-dimensional shape measurement with inner shifting-phase fringe projection profilometry[J]. *Chinese Optics Letters*, 2022, 20(11):112601.

[6] LU L, WU Z, ZHANG Q, *et al*. High-efficiency dynamic three-dimensional shape measurement based on misaligned gray-code light[J]. *Optics and Lasers in Engineering*, 2022, 150:106873.

[7] 冯维, 徐仕楠, 王恒辉, 等. 逐像素调制的高反光表面三维测量方法[J]. 中国光学(中英文), 2022, 15(3): 488-497.

FENG W, XU SH N, WANG H H, *et al*. Three-dimensional measurement method of highly reflective surface based on per-pixel modulation[J]. *Chinese Optics*, 2022, 15(3): 488-497.

[8] QIAO N, ZHANG F. Method for reducing phase errors due to CCD nonlinearity[J]. *Optik - International Journal for Light and Electron Optics*, 2016, 127(13): 5207-5210.

[9] LIU H, MA H, TANG Q, et *al*. Investigation of noise amplification questions in satellite jitter detected from CCDs' parallax observation imagery: A case for 3 CCDs[J]. *Optics Communications*, 2022, 503: 127422.

[10] XUE X, ZHANG C, ZHAO J, *et al*. The influence of CCD undersampling on the encircled energy of SVOM-VT[C]//AOPC 2019: Space Optics, Telescopes, and Instrumentation. SPIE, 2019, 11341: 23-35.

[11] DU Y ZH, FENG G Y, ZHANG K, *et al*. Effect of CCD nonlinearity on wavefront detection by shearing interferometry[J]. *High Power Laser and Particle Beams*, 2010, 22(8): 1775-1779.

In Press

[12] 程书博, 张惠颌, 王哲斌, 等. 科学级光学 CCD 非线性特性测试[J]. 光学学报, 2012, 32(4): 39-44.

CHENG S, ZHANG H, WANG Z, *et al*. Nonlinearity property testing of the scientific grade optical CCD[J]. *Acta Optica Sinica*, 2012, 32(4): 39-44. (in Chinese)

[13] 乔闹生, 孙萍. CCD 非线性效应对双频光栅三维面形测量的影响[J]. 中国光学(中英文), 2021, 14(3): 661-669.

QIAO N S, SUN P. Influence of CCD nonlinearity effect on the three-dimensional shape measurement of dual frequency grating[J]. *Chinese Optics*, 2021, 14(3): 661-669.

[14] LI J, SU X Y, GUO L R. Improved Fourier-transform profilometry for the automatic measurement of 3-dimensional object shapes[J]. *Optical Engineering*, 1990, 29(12): 1439-1444.

[15] QIAO N S. Effect of CCD nonlinearity on spectrum distribution[J]. *Optik - International Journal for Light and Electron Optics*, 2016, 127 (20): 8607-8612.

[16] WANG Y, LIN B. A fast and precise three-dimensional measurement system based on multiple parallel line lasers[J]. *Chinese Physics B*, 2021, 30: 024201.

[17] SUN J, ZHANG Q. A 3D shape measurement method for high-reflective surface based on accurate adaptive fringe projection[J]. *Optics and Lasers in Engineering*, 2022, 153: 106994.

[18] 曹智睿. 基于相移条纹投影的动态 3D 测量误差补偿技术[J]. 中国光学(中英文), 2023, 16(1): 184-192.

CAO ZH R. Dynamic 3D measurement error compensation technology based on phase-shifting and fringe projection[J]. *Chinese Optics*, 2023, 16(1): 184-192.

[19] 乔闹生, 尚雪. 非线性系统中双频光栅相位测量[J]. 中国光学(中英文), 2023, 16(3): 726-732.

QIAO N SH, SHANG X. Phase measurement with dual-frequency grating in nonlinear system[J]. *Chinese Optics*, 2023, 16(3): 726-732.

[20] 曹智睿. 基于相移条纹投影的动态 3D 测量误差补偿技术[J]. 中国光学(中英文), 2023, 16(1):184-192.

in press

CAO ZH R. Dynamic 3D measurement error compensation technology based on phase-shifting and fringe projection[J]. *Chinese Optics*, 2023, 16(1):184-192.

Author biographies:

QIAO Nao-sheng (1971-), Ph.D, Professor, International College, Hunan University of Arts and Science. His research interests are optical information processing. E-mail: naoshengqiao@163.com

in press